

Explicit dynamic finite element analysis of an automated grasping process using highly damped compliant fingers

Kok-Meng Lee^{a,b}, Chih-Hsing Liu^{c,*}

^a Woodruff School of Mechanical Engineering, Georgia Inst. of Tech., Atlanta, GA, USA

^b School of Mechanical Engineering, Huazhong University of Science and Technology, Wuhan, China

^c Singapore Institute of Manufacturing Technology, 638075 Singapore, Singapore

ARTICLE INFO

Keywords:

Compliant finger
Compliant mechanism
Explicit dynamic finite element
FEA
Multibody dynamics
Robotic hand

ABSTRACT

This paper has been motivated by the need to reduce the number of live animal tests in the development of an automated live-bird transfer system (LBTS) for the poultry meat-processing industry. Simulation-based models have been developed, which carefully address key engineering issues prior to live animal tests so that physical experiments can be focused on understanding reflex issues such as fear and escape behavior. To gain insights into the effects of operational timing on the LBTS handling performance, the multibody dynamics is modeled numerically based on the method of explicit dynamic finite element analysis (FEA) using off-the-shelf FEA packages. The findings also offer information on contact forces and their locations acting on the object's body and legs by the compliant fingers and grippers respectively for optimizing designs and avoiding damage to the object. Specifically, this paper discusses computational issues such as time-step considerations and highly damped behavior of compliant fingers when modeling using dynamic FEA methods. The FEA model has been validated by comparing simulated handling of an ellipsoidal object by a pair of robotic hands with multiple compliant fingers against published experimental data. It is expected that the FEA-based method presented here can be extended to a spectrum of applications where flexible multibody dynamics involving large deformable contacts and highly damped behaviors plays an important role.

© 2012 Elsevier Ltd. All rights reserved.

1. Introduction

Flexible multibody dynamic systems (FMDS) are widely used in the food processing industry to transfer input force, displacement and energy through elastic deformation of compliant components and/or joint-less structures. In poultry processing plants, for example, mechanical transferring of live products from moving conveyors to a production line must accommodate a limited range of sizes/shapes and natural reactions without causing damage [1], where the design of compliant fingers for automated handling at production rate is a fundamental task. Unlike a static structure, both the geometric and operating parameters of FMDS must be evaluated during design. Motivated by the need to develop a simulation-based technique for identifying key parameters of an FMDS prototype before engaging live products in experiments, this paper presents a numerical model using a general-purpose explicit finite element analysis (FEA) solver, LS-DYNA. As will be shown, the dynamic FEA provides a good understanding of the operational parametric effects on the handling performance.

* Corresponding author.

E-mail addresses: kokmeng.lee@me.gatech.edu (K.-M. Lee), chliu@simtech.a-star.edu.sg, chihhsing.liu@gmail.com (C.-H. Liu).

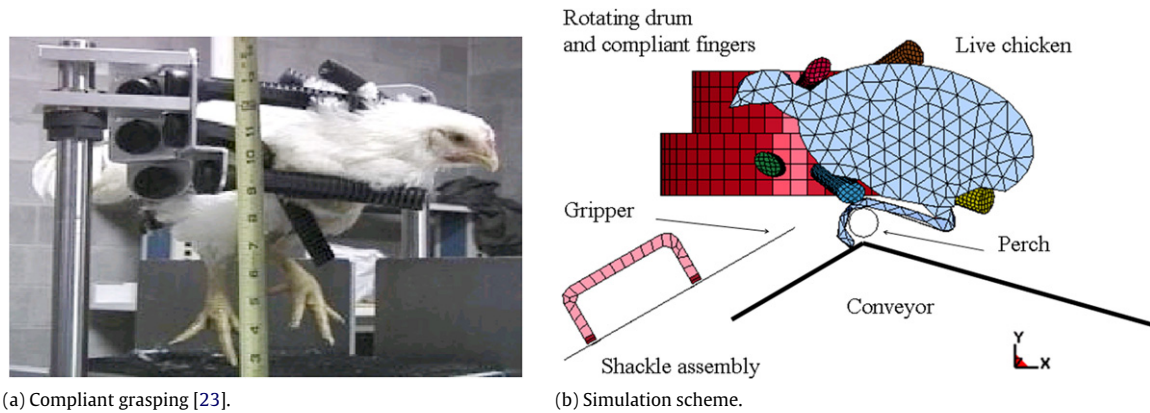


Fig. 1. Compliant grasping of a live bird transfer system (LBTS).

Compliant fingers have many advantages (such as being lightweight, having no relative moving parts and being relatively less expensive to manufacture) as compared to graspers [2–4] made up of rigid elements with active joints. The geometrical formulation for characterizing the large deflection of a flexible beam can be found in [5]; its cumbersome derivation of elliptical integrals, however, limits its applications to a geometrically simple beam subjected to a known load. Pseudo-rigid-body models [6,7] which approximate flexible members as rigid links with torsion pin-joints are also commonly used to find the end-point deflection of the beam. To predict the deflected shape of the entire link, Yin and Lee [8] extended their 2D flexible finger model [9] to analyze grasping of an elliptical object (geometrically modeling a bird body). Several other improved analytical models [10,11] to predict the contact force and deflected shape of a compliant finger have also been developed. These studies generally modeled the finger as a 2D beam, and analyzed the finger dynamics quasi-statically without considering its damping effect. While these lumped-parameter models have been found useful to reduce the number of hardware/software configurations to be tested, they are inadequate to analyze the dynamic response of the FMDS involving complex 3D geometries with large deformation and contact nonlinearity.

FEA has been increasingly used to analyze FMDS because of its capabilities to handle complex geometries and boundary conditions. Applications include impact and penetration analyses of fuselage-like structures [12], crash simulations of automobiles [13,14], bird-strike simulations of aeronautic structures [15], and dynamic analyses of rigid mechanisms mounted on flexible structures [16], and more recently FEA of motor rotor/spindle assembly [17] and a numerical study of penetration into reinforced concrete targets [18].

However, a tradeoff between computation time and numerical stability has been a persistent challenge to high-fidelity simulation. Dynamic FEA involves time-integration, which can be broadly classified into implicit and explicit methods. Implicit methods are stable for linear and many nonlinear problems but computationally more expensive than explicit methods which, unlike the former, do not require a stiffness matrix inversion in each time-step. An explicit method, however, is only stable when its time-step is smaller than a critical size known as the Courant–Friedrichs–Levy (CFL) condition [19,20]. Many studies [21,22] were proposed to discuss the stability problems of explicit methods. Because of these challenges, most existing FEA-based design methods evaluate geometrical parameters (such as size and shape) under stress, strain or displacement constraints. For industrial automation, synchronization of speeds (or transfer-rate) among different processes under a set of trajectory constraints introduces additional operational parameters to be evaluated.

The remainder of this paper offers the following:

- (1) In the context of an automated grasping process using highly damped compliant fingers, two 3D modeling issues for simulating multibody system dynamics are addressed; computational time-step and damped behavior of compliant fingers. The FEA models are validated by comparing simulated results against published experimental data.
- (2) The method for simulating the grasping of an ellipsoidal object by a mechanical hand consisting of multiple compliant fingers is presented. Unlike previous studies [8,9] where a 2D ellipse is used to model the geometry of a biological product (such as chicken), the geometrical model considered here is a 3D multibody system with relatively complete details; for example, including the legs and head of the chicken.
- (3) As an illustrative example, the effects of several key operating parameters on the dynamic grasping performance of the multibody system are investigated. The findings offer a means to predict the locations at which the compliant fingers act on the object body being grasped and gripping forces on the legs.

2. Numerical modeling of compliant grasping

To allow for a limited range of size/shape variations, highly damped rubber fingers are commonly used to handle live products. The compliant grasping problem is best illustrated in the context of a practical application based on a live bird transfer system (LBTS) [1,23] shown in Fig. 1. In operation, live birds are fed in a single file on a conveyor toward a pair of

rotating drums with compliant fingers designed to cradle the bird by its body. The two drums, rotating at the same speed but in the opposite direction, move the bird forward with its feet on the conveyor. While the fingers constrain its body, the conveyor inclines downward allowing the bird to extend its legs freely with the conveyor. As the bird's natural reflex is to maintain its stability by gripping on circular perch-bars (specifically designed on the moving conveyor), both legs of the bird can be manipulated by appropriately controlling the drum speed with respect to the conveyor speed. Once both legs are gripped, the bird is inverted with the shackle for transferring to a production line. The success of the automated LBTS depends on the optimal timing of rotating compliant fingers relative to the conveyor speed and the accurate presentation of the shackle for gripping the legs.

2.1. Basic formulations for explicit dynamic FEM

FEM simulates physical phenomena by converting a continuum into a discrete domain (nodes and elements). The discrete equations of motion for the explicit dynamic FEA can be derived from the work balance contributed by the external load, inertial and viscous effects, and strain energy [20]. For a single element subjected to body force, surface traction, and point load, the work balance of the element (with density ρ , viscous damping coefficient c , volume V , and surface S) is given by Eq. (1):

$$\int \{\delta u\}^T \{f\} dV + \int \{\delta u\}^T \{t\} dS + \sum_{i=1}^n \{\delta u\}_i^T \{p\}_i = \int (\{\delta u\}^T \rho \{\ddot{u}\} + \{\delta u\}^T c \{\dot{u}\} + \{\delta \varepsilon\}^T \{\sigma\}) dV \tag{1}$$

where the first, second and third terms on the left hand side denote the work done by the body force $\{f\}$, surface traction $\{t\}$ and the concentrated load $\{p\}$ respectively; whereas the first, second and third terms on the right hand side denote the work done by inertial effect, viscosity, and strain energy respectively; the notation $\{\}$ represents a vector; $\{\delta u\}$ is the virtual displacement; $\{\delta \varepsilon\}$ is the corresponding strain to the virtual displacement; and $\{u\}$ is the displacement which is function of space and time.

The displacement $\{u\}$ over an element can be represented by the interpolating functions and nodal degree-of-freedom (DOF) as in Eq. (2):

$$\{u\} = [N]\{x\} \tag{2}$$

where the space-dependent interpolation (or shape) function matrix $[N]$ can be determined according to the element types; and $\{x\}$ is the nodal DOF dependent on time only. With the aid of interpolation functions, strain and stress are given by Eq. (3a) and (3b) respectively.

$$\{\varepsilon\} = [B]\{x\}; \tag{3a}$$

$$\{\sigma\} = [E]\{\varepsilon\} = [E][B]\{x\} \tag{3b}$$

where $[B]$ is a strain-displacement matrix (space derivative of the interpolation function matrix $[N]$); and $[E]$ is a stress-strain matrix. With Eqs. (2) and (3a), (3b), Eq. (1) can be rewritten as (4) in terms of element mass, damping, and stiffness matrices as well as the external load, which are denoted by $[m]$, $[c]$, $[k]$ and $\{r_{ext}\}$ respectively in Eqs. (4a)–(4d):

$$[m]\{\ddot{x}\} + [c]\{\dot{x}\} + [k]\{x\} = \{r_{ext}\} \tag{4}$$

$$[m] = \int \rho [N]^T [N] dV \tag{4a}$$

$$[c] = \int c [N]^T [N] dV \tag{4b}$$

$$[k] = \int [B]^T [E] [B] dV \tag{4c}$$

$$\{r_{ext}\} = \int [N]^T \{f\} dV + \int [N]^T \{t\} dS + \sum_{i=1}^n \{p\}_i. \tag{4d}$$

By assembling the above element matrices, the equation of motion for the whole domain being analyzed is given by Eq. (5):

$$[M]\{\ddot{X}\} + [C]\{\dot{X}\} + [K]\{X\} = \{F\} \tag{5}$$

where $[M]$, $[C]$, and $[K]$ are the global mass, damping, and stiffness matrices respectively; and $\{X\}$ and $\{F\}$ are the global nodal DOF and load vectors respectively. In this paper, the numerical packages ANSYS will be used to create the discrete domain $\{X\}$, and LS-DYNA (which is an explicit time integration solver) will be used to solve the equation of motion.

2.2. Critical time-step

Explicit time-integration methods for dynamic FEA determine the unknowns for the next time-step in terms of quantities computed at the current or previous time-step. While computationally efficient, the explicit method requires the time-step Δt to satisfy the CFL condition (6) in order to ensure numerical stability [20,24].

$$\Delta t \leq \Delta t_c = L_e/c_w \tag{6}$$

where Δt_c is the critical time-step; L_e is the characteristic length; and c_w is the wave propagation speed. In an explicit FEA, Δt must be sufficiently small so that the wave cannot propagate across more than one element within each time-step. The critical time-step depends on material properties as well as element size and shape. The detailed formulation of Δt_c for different element types can be found in [24]. For numerical stability, the critical time-step must be calculated at each time instant for each element (Δt_{ci} , $i = 1 \sim n$, where n is element number). The numerical time-step is the smallest value in the global analysis domain, and scaled by a scalar parameter a (between 0 and 1; $a = 0.9$ is used in this paper) as given in (7):

$$\Delta t_{num} = a \times \min\{\Delta t_1, \Delta t_2, \dots \Delta t_n\}. \tag{7}$$

Eq. (7) implies the numerical time-step is determined by the smallest element in the FEM model for a specified material. A well-planned uniform mesh is a general guideline to reduce the computational time (increase the critical time-step) in an explicit dynamic FEA.

2.3. Damping modeling

The damping behavior of the compliant finger is modeled using Rayleigh’s proportional damping:

$$[C] = \alpha[M] + \beta[K] \tag{8}$$

where the mass and stiffness matrices, $[M]$ and $[K]$, can be formulated once the element types are defined; and α and β are the mass and stiffness proportional damping coefficients respectively. The relative effect of the damping coefficients on the damping ratio ζ can be illustrated with a classical single-DOF system (mass m , spring k and damper c). Using (8), the damping ratio ζ can be written in terms of the natural frequency ω_n :

$$\zeta = (\alpha/\omega_n + \beta\omega_n)/2. \tag{9}$$

For structures vibrating at low frequency, the stiffness proportional term β in (8) can be neglected [20]; and the mass proportional term α can be determined experimentally. Unlike a lightly damped case where the damping ratio can be identified from measured overshoots using a lumped parameter approach (for example, the log decrement method), the α coefficient of a highly damped continuum structure is determined here by a coupled method [25] combining explicit dynamic FEA and experimentally obtained impulse responses. This coupled method numerically searches for the mass proportional damping coefficient α of the continuum structure until a match between experimental data and the simulated response to an impulsive load is found. Then, the damping coefficient α can be further used as the input parameter in the following dynamic FEA

2.4. Contact model

For dynamic problems involving deformable contacts, the load vector $\{F\}$ in Eq. (5) includes forces at the contact interface. Formulated as a displacement constraint on the discretized nodes, the penalty method in LS-DYNA [24] is applied to simulate the contact. The distance between two particles can be expressed in terms of a gap function g_n ; g_n greater than, equal to, or less than zero denotes when two points are not in contact, at contact, or penetrate each other respectively. Physically, the penetration is invalid since two bodies cannot move into each other. However, a small penetration is necessary numerically and assumed in the penalty method in order to model the normal interface force f_n [24]:

$$f_n = -k_n g_n \quad \text{where } k_n = \begin{cases} s_f BA^2 & \text{for solid element} \\ \frac{V}{\max(\text{shell_diagonal})} s_f BA & \text{for shell element.} \end{cases} \tag{10}$$

In Eq. (10), the normal interface force f_n is proportional to g_n in terms of the penalty (interface) stiffness k_n , in which B is the bulk modulus (function of elastic modulus and Poisson ratio); A and V are the area and volume (of the element) in contact; and s_f is a scale factor (the suggest value is 1). Once the normal force is obtained, the Coulomb friction formulation is used to calculate the lateral friction force.

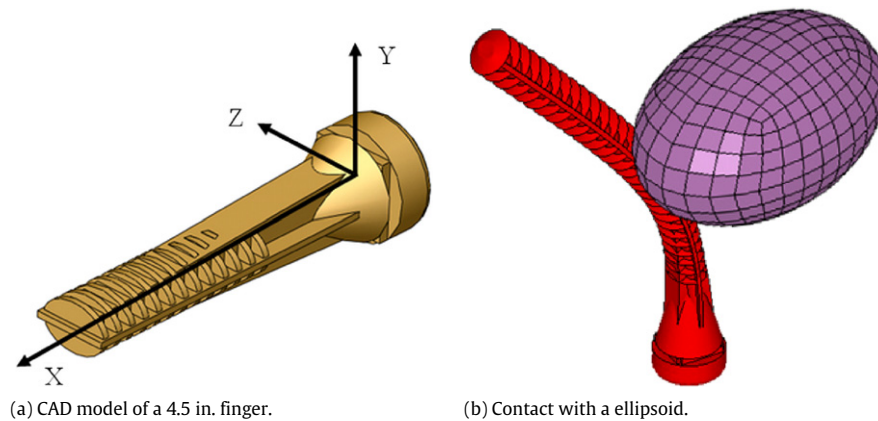


Fig. 2. Compliant rubber fingers finger.

3. Validation and illustrative examples

In the interests of reducing the number of live animal tests in the development of an LBTS with highly damped compliant fingers, the FEA-based method described in Section 2 is employed here to model the dynamic behavior of the finger where published experimental data are available for validation. Specifically, the following are discussed:

- (1) The effects of computational time-step and highly damped behavior on the modeling of compliant fingers are discussed.
- (2) For validation, the dynamics of an existing grasper [26,27] similar to that shown in Fig. 1(b) except that the object is an ellipsoidal football were simulated, where experimental results in [28] provide a basis for comparison.
- (3) The grasping performance of an LBTS was investigated to determine the optimal motion trajectories for operating the multibody system.

Detailed description of the corresponding element types used in above analyses can be found in [29].

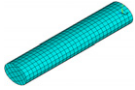
3.1. Modeling of highly damped compliant finger

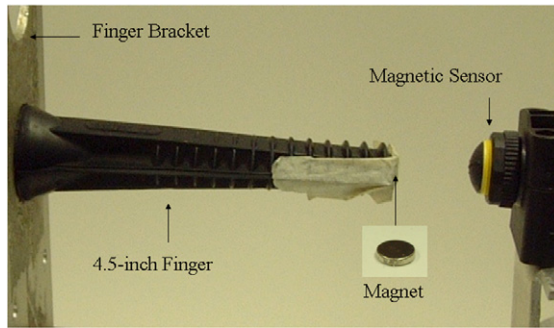
As detailed in Fig. 2(a), the compliant finger consists of evenly-spaced elliptical ribs along with the reinforced structure making up of a thin horizontal plate, a cone and a rectangular section tapering from the fixed circular end (17.5 mm radius). The slot near the cylindrical base is reserved for mounting the finger onto the drum such that the finger rotates as a flexible cantilever beam with the drum. The finger is designed to bend easily in the XY plane but relatively rigid in other planes. Fig. 2(b) shows the flexible contact deformation of an 8 in. finger.

To illustrate the effects of geometrical complexity on the computational time-steps and the damping, Table 1 compares two different FE models of a 4.5 in. compliant finger used in the LBTS; a detailed model (DM) and a simplified model (SM) that has a constant elliptical cross-section. For low frequency applications, the stiffness proportional damping β in Eq. (8) was set to zero, and the mass proportional damping coefficients were determined using trial-and-error FEA simulations (based on SM and DM under different mass proportional damping coefficients) to match experimentally obtained impulse responses of the tip motion. The experimental setup for the impulse response is shown in Fig. 3(a), where the finger is clamped at the base; and a (4 mm-radius, 1.65 mm-thick) cylindrical permanent magnet is attached at the free-end such that the tip motion can be measured by a Banner S18MB magneto-resistive sensor. The mass proportional damping coefficient was found to be 260 s^{-1} and 180 s^{-1} for DM and SM respectively. The results are compared in Fig. 3(b), both showing over-damped responses. Some observations can be made from Table 1 and Fig. 3:

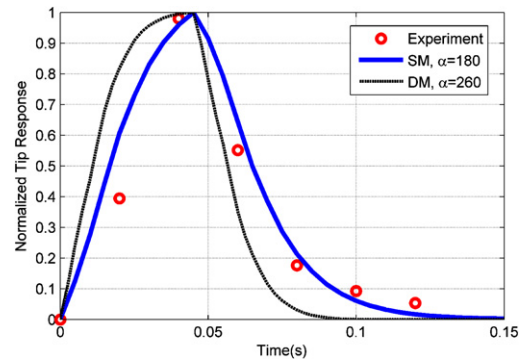
- (1) DM cannot be meshed with hexa elements because of its complex geometry. The average element length 2.8 mm is the maximum value to mesh DM in ANSYS. Small detailed features lead to non-homogeneously small element length. As the time-step is determined by the smallest element in the global analysis domain as given in Eq. (7), this leads to a large number of steps (18.36 times more than SM) to solve the same dynamic problem.
- (2) For each computational step, the global matrix size is $3n \times 3n$ where n is the number of nodes (each node with three degrees-of-freedom). So the actual computational time ratio of DM to SM is even larger than the step ratio (18.36).
- (3) DM (with ribs and stronger fixed end) is stiffer than SM. For the same α of 180 s^{-1} , SM exhibits an over-damped response while the DM appears under-damped. This is because their geometries are different, and thus their mass and stiffness matrices. DM with $\alpha = 260 \text{ s}^{-1}$ gives a similar over-damped tip response. The match between simulation and experiment for SM is better than DM.

Table 1
Detailed and simplified FEM models of the 4.5 in. compliant finger.

FEM models	Rubber $E = 6.1 \text{ MPa}$ $\nu = 0.49$ $\rho = 1000 \text{ kg/m}^3$	Element type Average length # of nodes # of elements	Time-step size ($\mu \text{ s}$) # steps to 0.2s Step ratio (relative to SM)
Detailed model (DM)		Tetra (Solid 168) 2.8 mm 36,782 23,147	0.22 909,091 18.36
Simplified model (SM)		Haxa (Solid 164) 4 mm 1080 725	4.04 49,505 1



(a) Experimental setup.



(b) 4.5 in. finger tip response.

Fig. 3. Damping modeling of a 4.5 in. compliant finger.

In summary, SM tolerates a larger time-step (thus faster computation) than the DM as expected. As SM overestimates the deflection/stress, it represents a conservative model and has been used in the subsequent simulation. The α value of the 4.5 in. finger is 180 s^{-1} . Following the same damping modeling procedure with SM, the α value of the 3 in. finger is found to be 600 s^{-1} .

3.2. Experimental validation

For validation, the experimental setup [28] shown in Fig. 4 was numerically simulated, where Fig. 4(a) are the encoder readings of the drums and the conveyor (same speed as pallet). Fig. 4(b)–(d) are three selected video snapshots illustrating the three tasks of the grasper. In this setup, the football was initially placed on the pallet moving at 0.457 m/s towards the rotating hands. Once the pallet reached $X = 0.142 \text{ m}$, it decelerated to 0.254 m/s while both robotic hands began to rotate from their initial positions at the same speed (20 rpm) but in opposite directions. The grasper configuration is given in Fig. 5 and Table 2, where A–E denote the finger number. The following assumptions are made in the simulation:

- (1) The football is homogeneous with density calculated from the weight divided by volume.
- (2) The football is transported along the centerline and thus, a half-symmetric model is used in the simulation.
- (3) The football, fingers and pallet surface are rubber materials. The static and dynamic friction coefficients [8] between them are 0.4 and 0.3 respectively.
- (4) All the motions follow step commands; the acceleration and deceleration effects in Fig. 4(a) are neglected.

The results (simulated using the SM finger model) are given in Fig. 6 with simulation parameters summarized in Table 2. Fig. 6(a) compares the Y displacement against published experimental results [28]. Fig. 6(b) displays a sequence of simulated snapshots which qualitatively agree with the experimental data. Both simulation and experimental results show that the compliant grasper successfully lifts the football off the pallet surface, and the duration of the lift (about 20 mm) is about 1s. The overall trend of the simulation closely follows the experiment. The simulation, however, estimates a larger maximum (about 2 mm) displacement than experimental data. This discrepancy may be contributed by two causes: The first is that the finger model (SM) neglects the rigs and the taper fixed-end section, and thus tends to predict a larger deflection and higher stresses. The second could be due to the oscillations in the experimental specified conveyor and drum velocities as shown in Fig. 4(a) whereas these specified velocities are ideal step response in the simulation.

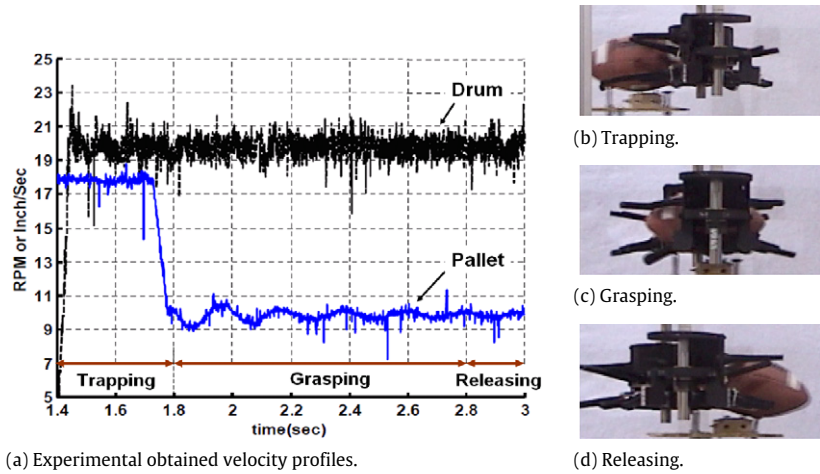


Fig. 4. Experiment of football handling [28].

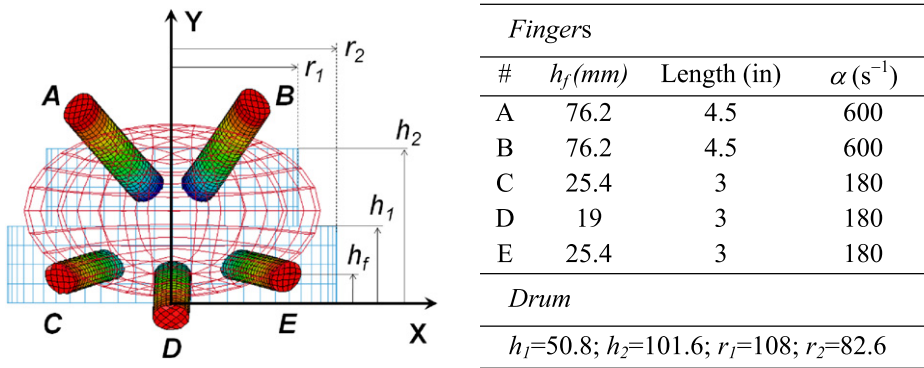


Fig. 5. Grasper configuration.

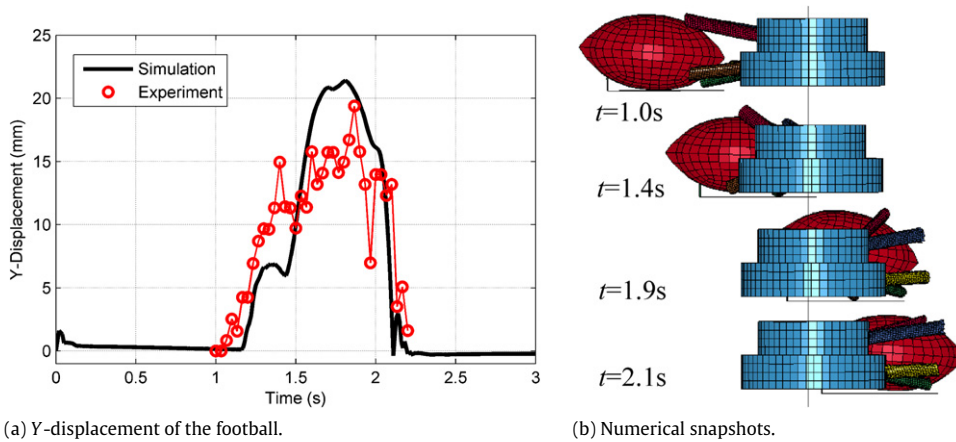


Fig. 6. Simulated responses of the football handling.

3.3. Illustrative application

With the FEA-based model validated using a football, the LBTs dynamics are further investigated using a detailed bird model as shown in Fig. 7. The geometrically detailed model provides a more realistic prediction of the contact locations,

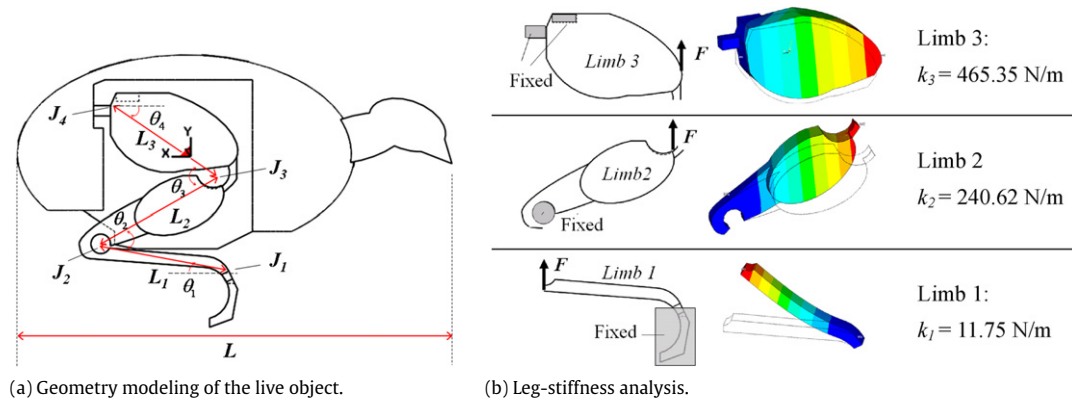


Fig. 7. Compliant chicken model.

Table 2
Simulation parameters of football handling.

Part	Material E (GPa); ν ; ρ (kg/m ³)	FEM element type # of element/nodes	Dimension (mm)
Football	Rubber 0.0061; 0.49; 275	Solid 164 512/677	488 × 264 × 264 (0.425 kg)
Drum	AL6061 69; 0.33; 2700	Shell 163 1271/1212	$h_1 = 50.8$; $h_2 = 101.6$ $r_1 = 108$; $r_2 = 82.6$
Pallet	Steel 210; 0.28; 7700	Shell 163 2/6	200 × 50
Fingers	Rubber 0.0061; 0.49 1000	Solid 164 A, B: 725; 1080 C, D, E: 500; 756	Fig. 5 Detailed configuration can be found in [26,27]

and additionally a better understanding on how the timing commands of the grasper motion relative to the conveyor speed would affect the leg and body motions during transfer.

Bird model

The bird model includes a half ellipsoid as bird body, a head, and a leg of three limbs connected with compliant joints. The leg model is connected with the ellipsoid at joint 4 as shown in Fig. 7(a), where L_i is the length of the i th limb; J_i and θ_i are the i th joint and i th angle between two limbs respectively; and L is the total length of the chicken. The dimensions (based on measurements of commercial meat chickens [30]) are summarized in Table 3. The characteristic dimensions of the bird are defined with respect to the geometric center of the ellipsoid. More detailed dimensions of the chicken model can be found in [27].

The force–displacement relationships of the compliant joints (between two adjacent limbs) are computed using nonlinear static FEA meshed with the 10-Node tetrahedral element (Solid 92). Each limb is fixed at one end and a known force is applied at the other end as illustrated in Fig. 7(b), which shows the loading boundary conditions, the deformation contours, and the corresponding equivalent stiffness for each limb.

Simulation Assumptions:

The following assumptions are made in modeling the chicken:

1. It has negligible time to react within the short cycle time and thus is modeled as a passive dummy.
2. It is modeled as a compliant mechanism (having no feather) with linear, homogeneous and isotropic rubber-like material (with density calculated from the average measured weight divided by the volume of the CAD modeled chicken).
3. It grips on the perch during the transfer process. The chicken-paw and the perch bar on conveyor are coupled and move simultaneously.

In addition, we further assume the followings.

4. The chicken, mechanical structures and associated boundary conditions are symmetric about the x - y plane (Fig. 8(a)). Thus, a half symmetric model is used to simulate the body-grasping and leg-gripping processes.
5. Damping effects are neglected except for highly damped compliant fingers [31].

Motion commands

Fig. 8(a) shows the plan view of the LBTS design, where the X - Z plane is symmetric about the centerline of the shackle so a half symmetric model is used in simulation. The sectional view at the symmetric plane and the trajectories of the input operating parameters are given in Fig. 8(b) illustrating the time sequence of the simulation which begins with an

Table 3
Geometric parameters of the compliant chicken model.

Body (Ellipsoid)	Semi-axes (mm): 97, 66, 57 Origin: geometric center of the ellipsoid Total length $L = 250$ mm		
Joint location (mm)	$J_1 (-24.72, -67.3, 40)$ fixed with the perch		
Dimension (mm):	$J_2 (49, -51.6, 40)$; circular hole (5.7, 10)		
Circular hole (radius, thickness)	$J_3 (-15.74, -10.74, 40)$; circular hole (10, 10)		
Brick (length, height, thickness)	$J_4 (43.37, 27.89, 35)$; brick (9.85, 7.52, 5.93), (13, 4.76, 5)		
Limb Length and thickness (mm)	L_1	75	20
	L_2	77	20 (upper limb), 10 (lower limb)
	L_3	71	10
Initial angle (°)	$\theta_1 = 10,$	$\theta_2 = 40,$	$\theta_3 = 65, \theta_4 = 35$

Table 4
Design analysis cases for different operating drum speeds (rpm).

Time (s)	Case A	Case B	Case C
0.00–0.55 (t_1)	35	45	45
0.55–0.85 (t_2)	35	45	20
0.85–1.10 (t_f)	35	45	40

Table 5
Material and FE model for grasping of live object.

Part	Material	E (GPa)	ν	ρ (kg/m ³)	Element type	# of elements	# of nodes	
Chicken	–	0.0061	0.49	1270	Solid 168	2233	4328	
Perch	AL6061	69	0.33	2700	Shell 163	144	156	
Shackle	Steel	210	0.28	7700	Shell 163			
Shackle base (for leg gripping)						405	537	
Shackle side holder						27	52	
Fingers & Drum	Same as Table 2 except finger E is 4.5 in. in this case							
Sum	–	–	–	–	–	7255	11,037	

incoming chicken (perching on circular bars) moving with the conveyor at speed V_c . The body-grasping and leg-gripping take place when the chicken passes through the compliant hands. The operating parameters are defined in Fig. 8(b) showing key instants critical to the processes:

- t_p : the perch arrives at the highest point of the conveyor path;
- t_s : the perch arrives at the gripper location; and
- t_f : the body of the leg-gripped chicken is released onto the shackle mechanism.

The interest here is to understand the effect of operating drum speeds and corresponding timing on the overall grasping performance.

Effect of rotational speeds

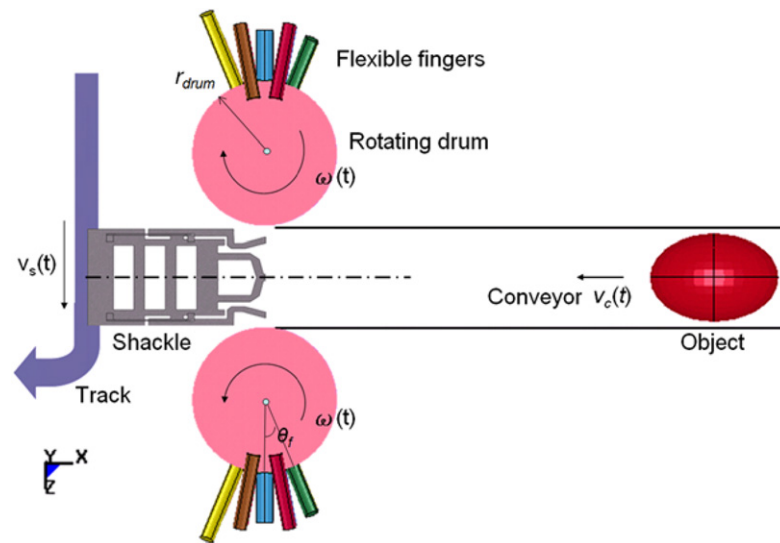
The effect of rotating hand speeds on the overall transfer performance was investigated by comparing three different cases of speed sequences given in Table 4. Because of high-damped flexible fingers with contact deformation, along with complex geometry, the multibody motion is a nonlinear function of time. High fidelity simulation will help predict the posture of the chicken as it moves through the fingers. To explore the nonlinear effect of drum speeds on the success of grasping the chicken, two additional instants (at which the drum changes its speed) are introduced:

- t_1 : the drums are temporarily slowed down, whereas
- t_2 : the drum speed is increased, and fingers push the chicken body onto the shackle.

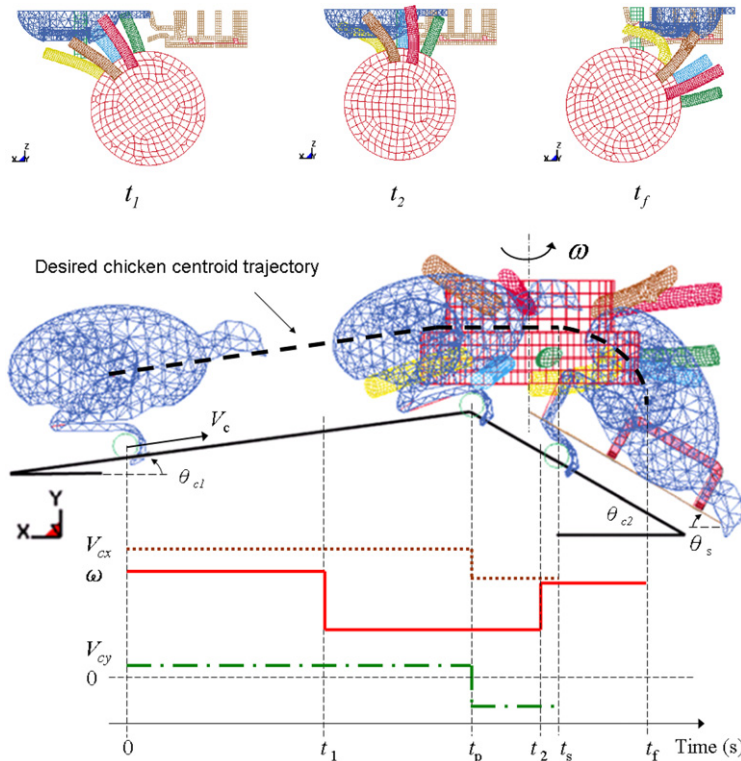
As shown in Table 4, Case C uses a sequence of three different speeds to account the nonlinear contact deformation, the results of which are compared against two constant drum-speed operations. The conveyor inclination θ_c also makes the problem more complex as it changes the object position in y -axis as well as the x and y -component speeds (V_{cx} and V_{cy}) while the compliant hand rotates (with speed ω) on the x - z plane. The FE model and corresponding boundary conditions are summarized in Tables 5 and 6, respectively.

Results and discussions

Simulation results are given in Figs. 9 and 10. Fig. 9 compares the three cases defined in Table 4, where snapshots in Fig. 9(a) are captured at $t_p = 0.7$ s and $t_f = 1.1$ s corresponding to body-grasping and leg-gripping respectively. In Fig. 9(a), the first two columns are plan- and side-views comparing the body-grasping at $t_p = 0.7$ s, whereas the last column compares



(a) plain view.

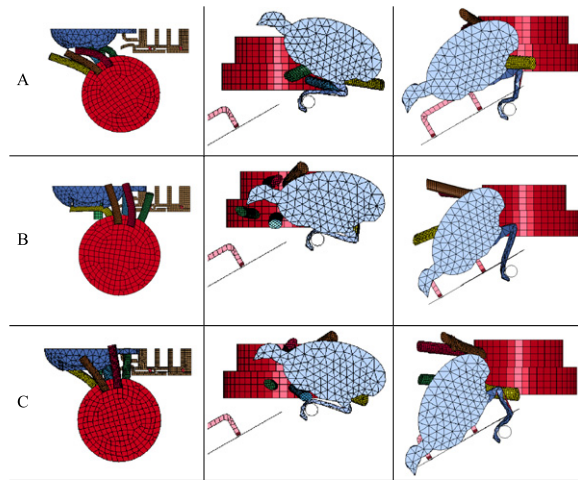


(b) Sectional view at the symmetric plane (half-symmetric model) and trajectories of the input operating parameters.

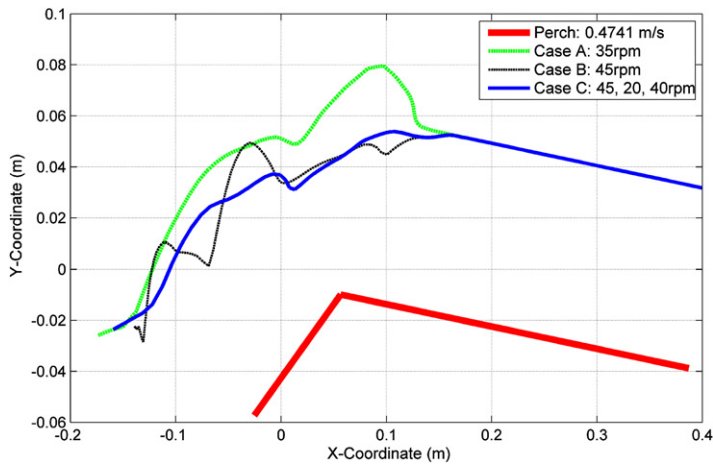
Fig. 8. Illustrative LBTS schematics.

the landing postures of the leg-gripped chicken at $t_f = 1.1$ s. Fig. 9(b) quantitatively compares the trajectories of the body-center with respect to that of the perch (top-center point). To compare the stresses acting on the legs, simulations assume that Joint 1 rigidly fixed on the perch bar; results are compared in Fig. 9(c). More detailed results for the optimal Case C are given in Fig. 10. The following are some observations drawn from these results:

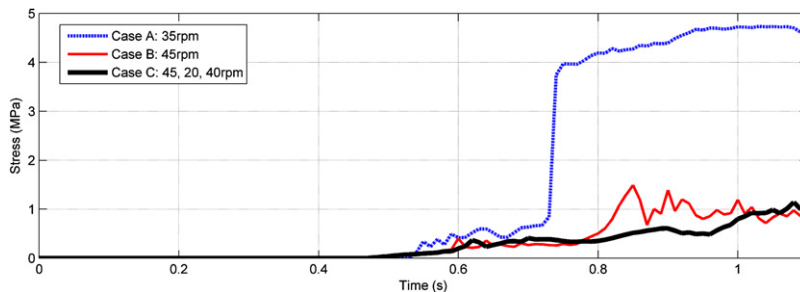
- The grasper motion in Cases A and B fails to cradle the chicken body; while the former is too slow and the latter is fast relative to conveyor speed. Several different values of constant drum speeds between 35 rpm and 45 rpm were



Plan view ($t_p=0.7s$) Side view ($t_p=0.7s$) Side view ($t_p=1.1s$)
 (a) Comparison of snapshots at $t_p = 0.7 s$ and $t_p 1.1 s$.



(b) Trajectories of the body with respect to the perch bar.



(c) Maximum stresses acting on the legs by the grippers.

Fig. 9. Comparison of the three cases (defined in Table 4).

experimentally evaluated. Although it is possible to find a *constant* drum speed at which the grasper can momentarily cradle the chicken, excessively large body momentum created by the high drum speed could “throw” its body resulting in excessive stresses on the legs gripped by the shackle. As compared in Fig. 9(c), the excessively high stresses on the legs in Case A indicate that the chicken legs will be pulled out of the shackle in practice. The relatively low but oscillatory stresses in Case B indicate that the fingers fail to cradle the chicken and have little effect on the leg-gripping.

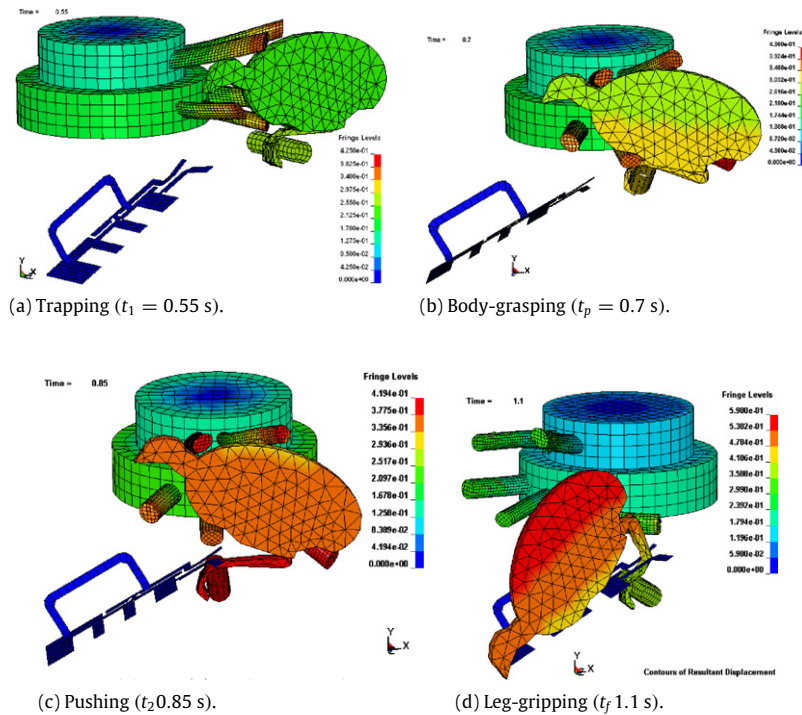


Fig. 10. Snapshots for selected instants for the optimal set of operating parameters (Case C).

Table 6
Boundary conditions for grasping of live object.

Parameters	Values
Origin	Drum bottom center
Initial position (m):	
Chicken	$x, y, z = 0.402, 0.032, 0.184$
Perch (top-center)	$x, y, z = 0.387, -0.039, 0.184$
Shackle	Gripper: $x, y, z = 0, -0.026, 0.130$ Fixed end: $x, y, z = -0.187, -0.135, 0.116, 0.184$ Initial angle: 32°
Drum speed	See Table 4
Conveyor angle	5° inclination, 30° declination acme: 50.8 mm (2 in.) from drum center
Conveyor speed (m/s):	0.4741 (18.67 inch/s)
0.0–0.7s	$V_{cx} = 0.4723, V_{cy} = 0.04132$
0.7–0.9s	$V_{cx} = 0.4105, V_{cy} = 0.23705$
Bird initial velocity (m/s)	0.4723 (x), 0.04132 (y)
Shackling time	$t = 0.9$ s, perch arrives shackling point
Gravity	9.81 m/s ² from $t = 0.9$ s (shackling time)
Static/Dynamic friction	0.4/0.3
Damping coefficient	3 in. finger: 600 s^{-1} ; 4.5 in. finger: 180 s^{-1}
Simulation time	1.1s

– Motivated by the results of the investigation with live chickens in [1] which experimentally determined the optimal drum speed for gripping both legs of the chicken to be about 20 rpm relative to a conveyor speed of 18 inches/second, these (along with the findings of Cases A and B) led to the design of Case C trajectory of non-constant drum speeds with an objective to find an optimal trade-off among several different performance measures including short cycle-time, fast body-grasping and successful leg-gripping. The high speed commands not only reduce the cycle time, but more importantly also minimize visual contact with the fingers before t_1 and the effects on leg-gripping by rapidly releasing the chicken from the fingers after t_2 , respectively. Unlike Cases A and B, Case C exhibits a smooth body trajectory and low (gradually increasing) stresses acting on the legs in Fig. 9(b) and 9(c); these predictions can be used as design criteria to determine the optimal set of speed commands. Fig. 10 shows several snapshots (captured at $t_1 = 0.55$ s, $t_p = 0.7$ s,

$t_2 = 0.85$ s and $t_f = 1.1$ s), which further illustrate the effects of the operating parameters for Case C on the successful body-grasping and leg-grasping processes.

4. Conclusion

A practical application using highly damped compliant fingers for handling of live objects at production rate has been illustrated. Two general-purpose FEA packages (ANSYS and LS-DYNA) that offer the advantages to handle complex geometries and boundary conditions have been employed in this study; specifically, modeling challenges involved in the simulations have been highlighted and addressed. Unlike previous studies using simple geometries and quasi-static models without considering damping of the finger, a more detailed chicken model including its legs and head has been developed to better understand the contact and dynamics of the leg/body motion during the automated grasping process. The FEA model has been validated by comparing simulated results of handling of a football (which is similar to the poultry body) by robotic hands with multiple compliant fingers against published experimental data. The geometrically detailed model provides a more realistic prediction of the contact locations, and additionally a better understanding on how the timing commands of the grasper motion relative to the conveyor speed would affect the leg and body motions during the transfer.

Acknowledgments

This work was jointly funded by the Georgia Agriculture Technology Research Program, the US Poultry and Egg Association, the Georgia Food Processing Advisory Council and the Georgia Food Industry Partnership.

References

- [1] K.-M. Lee, Design criteria for developing an automated live-bird transfer system, *IEEE Transactions on Robotics and Automation* 17 (4) (2001) 483–490.
- [2] G. Liu, J. Xu, X. Wang, Z. Li, On quality functions for grasp synthesis, fixture planning, and coordinated manipulation, *IEEE Transactions on Automation Science and Engineering* 1 (2) (2004) 146–162.
- [3] J. Xu, Z. Li, A kinematic model of finger gaits by multifingered hand as hybrid automaton, *IEEE Transactions on Automation Science and Engineering* 5 (3) (2008) 467–479.
- [4] L. Wang, L. Ren, J.K. Mills, W.L. Cleghorn, Automated 3-D micrograsping tasks performed by vision-based control, *IEEE Transactions on Automation Science and Engineering* 7 (3) (2010) 417–426.
- [5] R. Frisch-Fay, *Flexible Bars*, Butterworth, London, 1962.
- [6] L.L. Howell, A. Midha, T.W. Norton, Evaluation of equivalent spring stiffness for use in a pseudo-rigid-body model of large-deflection compliant mechanisms, *ASME Journal of Mechanical Design* 118 (1996) 126–131.
- [7] A. Midha, L.L. Howell, T.W. Norton, Limit positions of compliant mechanisms using the pseudo-rigid-body model concept, *Mechanism and Machine Theory* 35 (2000) 99–115.
- [8] X. Yin, K.-M. Lee, Modeling and analysis of grasping dynamics for high speed transfer of live birds, in: *Proc. of the 2nd IFAC Conf. on Mechatronic Systems*, Berkeley, California, 2002, pp. 719–724.
- [9] K.-M. Lee, J. Joni, X. Yin, Compliant grasping force modeling for handling of live objects, in: *ICRA2001*, Seoul, Korea, 2001, pp. 1059–1064.
- [10] C.-C. Lan, K.-M. Lee, An analytical contact model for design of compliant fingers, *ASME Journal of Mechanical Design* 130 (1) (2008).
- [11] Q. Li, K.-M. Lee, An adaptive meshless method for modeling large mechanical deformation and contacts, *ASME Journal of Applied Mechanics* 75 (4) (2008).
- [12] N.F. Knight, N. Jaunky, R.E. Lawson, D.R. Ambur, Penetration simulation for uncontained engine debris impact on fuselage-like panels using LS-DYNA, *Finite Elements in Analysis and Design* 36 (2) (2000) 99–133.
- [13] G.R. Consolazio, J.H. Chung, K.R. Gurley, Impact simulation and full scale crash testing of a low profile concrete work zone barrier, *Computers & Structures* 81 (13) (2003) 1359–1374.
- [14] L. Kwasniewski, C. Bojanowski, J. Siervogel, J.W. Wekezer, K. Cichocki, Crash and safety assessment program for paratransit buses, *International Journal of Impact Engineering* 36 (2) (2009) 235–242.
- [15] A.G. Hanssen, Y. Girard, L. Olovsson, T. Berstad, M. Langseth, A numerical model for bird strike of aluminium foam-based sandwich panels, *International Journal of Impact Engineering* 32 (7) (2006) 1127–1144.
- [16] H.-K. Sun, C.-G. Chen, H.-P. Wang, Dynamic analysis of rigid-body mechanisms mounted on flexible support structures – spatial case, *Journal of the Chinese Society of Mechanical Engineers* 28 (6) (2007) 585–591.
- [17] M.-F. Chen, W.-L. Huang, Investigation into the finite element modeling and dynamic characteristics of the assembly of spindle and motor rotor, *Journal of the Chinese Society of Mechanical Engineers* 32 (3) (2011) 257–266.
- [18] Y. Liu, F. Huang, A. Ma, Numerical simulations of oblique penetration into reinforced concrete targets, *Computers & Mathematics with Applications* 61 (8) (2011) 2168–2171.
- [19] R. Mullen, T. Belytschko, An analysis of an unconditionally stable explicit method, *Computers & Structures* 16 (6) (1983) 691–696.
- [20] R.D. Cook, D.S. Malkus, M.E. Plesha, R.J. Witt, *Concepts and Applications of Finite Element Analysis*, fourth ed., Wiley, 2001.
- [21] B.P. Sommeijer, Increasing the real stability boundary of explicit methods, *Computers & Mathematics with Applications* 19 (6) (1990) 37–49.
- [22] C.D. Acosta, C.E. Mejía, Stabilization of explicit methods for convection diffusion equations by discrete mollification, *Computers & Mathematics with Applications* 55 (3) (2008) 368–380.
- [23] A.B. Webster, K.-M. Lee, Automated shackling: how close is it? *Poultry International* 42 (4) (2003) 28–36.
- [24] LS-DYNA theory manual (compiled by Journal O. Hallquist), Livermore Software Technology Corporation, 2006.
- [25] C.-H. Liu, K.-M. Lee, Dynamic modeling of damping effects in highly damped compliant fingers for applications involving contacts, *ASME Journal of Dynamic Systems, Measurement, and Control* 134 (1) (2012).
- [26] C.-H. Liu, K.-M. Lee, Explicit finite element analysis of a flexible multibody dynamic system with highly damped compliant fingers, in: *2010 IEEE/ASME Int. Conf. on Advanced Intelligent Mechatronics*, Montreal, Canada, 2010, pp. 43–48.
- [27] C.-H. Liu, A finite element based dynamic modeling method for design analysis of flexible multibody systems, Ph.D. Dissertation, Georgia Institute of Technology, 2010.
- [28] X. Yin, Modeling and analysis of grasping dynamics for high speed transfer of live birds, Ph.D. Dissertation, Georgia Institute of Technology, 2003.
- [29] ANSYS element reference, Release 12, ANSYS Inc.
- [30] M.D. Summer, Design algorithm of a novel computer controlled gripper for a live bird transfer system, M.S. Thesis, Georgia Institute of Technology, 2002.
- [31] K.-M. Lee, On the development of a compliant grasping mechanism for on-line handling of live objects, part I: analytical model, in: *IEEE/ASME Int. Conf. on Advanced Intelligent Mechatronics*, Atlanta, GA, 1999, pp. 354–359.